

GENETICS

CRISPR-Cpf1 correction of muscular dystrophy mutations in human cardiomyocytes and mice

Yu Zhang,^{1,2,3*} Chengzu Long,^{1,2,3††} Hui Li,^{1,2,3} John R. McAnally,^{1,2,3} Kedryn K. Baskin,^{1,2,3} John M. Shelton,⁴ Rhonda Bassel-Duby,^{1,2,3} Eric N. Olson¹

2017 © The Authors, some rights reserved; exclusive licensee American Association for the Advancement of Science. Distributed under a Creative Commons Attribution NonCommercial License 4.0 (CC BY-NC).

Duchenne muscular dystrophy (DMD), caused by mutations in the X-linked dystrophin gene (*DMD*), is characterized by fatal degeneration of striated muscles. Dilated cardiomyopathy is one of the most common lethal features of the disease. We deployed Cpf1, a unique class 2 CRISPR (clustered regularly interspaced short palindromic repeats) effector, to correct *DMD* mutations in patient-derived induced pluripotent stem cells (iPSCs) and *mdx* mice, an animal model of DMD. Cpf1-mediated genomic editing of human iPSCs, either by skipping of an out-of-frame *DMD* exon or by correcting a nonsense mutation, restored dystrophin expression after differentiation to cardiomyocytes and enhanced contractile function. Similarly, pathophysiological hallmarks of muscular dystrophy were corrected in *mdx* mice following Cpf1-mediated germline editing. These findings are the first to show the efficiency of Cpf1-mediated correction of genetic mutations in human cells and an animal disease model and represent a significant step toward therapeutic translation of gene editing for correction of DMD.

INTRODUCTION

Duchenne muscular dystrophy (DMD) is an X-linked recessive disease caused by mutations in the gene coding for dystrophin, which is a large cytoskeletal protein essential for the integrity of muscle cell membranes (1). DMD causes progressive muscle weakness, culminating in premature death by the age of 30 years, generally from cardiomyopathy. There is no effective treatment for this disease. Numerous approaches to rescue dystrophin expression in DMD have been attempted, including delivery of truncated dystrophin or utrophin by recombinant adeno-associated virus (AAV) (2, 3) and skipping of mutant exons with antisense oligonucleotides and small molecules (4). However, these approaches cannot correct *DMD* mutations or permanently restore dystrophin expression.

The CRISPR (clustered regularly interspaced short palindromic repeats) system functions as an adaptive immune system in bacteria and archaea that defends against phage infection (5). In this system, an endonuclease is guided to specific genomic sequences by a single guide RNA (sgRNA), resulting in DNA cutting near a protospacer adjacent motif (PAM) sequence. The CRISPR-Cas (CRISPR-associated proteins) system represents a promising approach for correction of diverse genetic defects (6–12). However, many challenges remain to be addressed. For example, *Streptococcus pyogenes* Cas9 (SpCas9), currently the most widely used Cas9 endonuclease, has a G-rich PAM requirement (NGG) that excludes genome editing of AT-rich regions (13). Additionally, the large size of SpCas9 reduces the efficiency of packaging and delivery in low-capacity viral vectors, such as AAV vectors. The Cas9 endonuclease from *Staphylococcus aureus* (SaCas9), although smaller in size than SpCas9, has a PAM sequence (NNGRRT) that is longer and more complex, thus limiting the range of its genomic targets (13). Smaller

CRISPR enzymes with greater flexibility in recognition sequence and comparable cutting efficiency would facilitate precision gene editing, especially for translational applications.

Recently, a new RNA-guided endonuclease, named Cpf1 (CRISPR from *Prevotella* and *Francisella* 1), was shown to be effective in mammalian genome cleavage (14–18). Cpf1 has several unique features that expand its genome editing potential: (i) Cpf1-mediated cleavage is guided by a single and short crRNA (abbreviated as gRNA), whereas Cas9-mediated cleavage is guided by a hybrid of CRISPR RNA (crRNA) and a long trans-activating crRNA (tracrRNA) (19). (ii) Cpf1 prefers a T-rich PAM at the 5' end of a protospacer, whereas Cas9 requires a G-rich PAM at the 3' end of the target sequence. (iii) Cpf1-mediated cleavage produces a sticky end distal to the PAM site, which activates DNA repair machinery, whereas Cas9 cutting generates a blunt end. (iv) Cpf1 also has ribonuclease activity, which can process precursor crRNAs to mature crRNAs (14, 20). Like Cas9, Cpf1 binds to a targeted genomic site and generates a double-stranded break, which is then repaired either by nonhomologous end joining (NHEJ) or by homology-directed repair (HDR) if an exogenous template is provided. Although Cpf1 has been shown to be active in mammalian genome editing (14–17), its potential usefulness for correction of genetic mutations in mammalian cells and animal models of disease has yet to be demonstrated.

Previously, we and others used CRISPR-Cas9 to correct the *DMD* mutation in mice and human cells (7, 9, 10, 21–23). Here, we show that Cpf1 provides a robust and efficient RNA-guided genome editing system that can be used to permanently correct *DMD* mutations by different strategies, thereby restoring dystrophin expression and preventing progression of the disease. These findings provide a new approach for the permanent correction of human genetic mutations.

RESULTS

Correction of DMD iPSC-derived cardiomyocytes by Cpf1-mediated genome editing

Exon deletions preceding exon 51 of the human *DMD* gene, which disrupt the open reading frame (ORF) by juxtaposing out-of-frame exons, represent the most common type of human DMD mutation (24). Skipping of exon 51 can, in principle, restore the DMD ORF in 13% of DMD patients with exon deletions (25). To test the potential of Cpf1

¹Department of Molecular Biology, University of Texas Southwestern Medical Center, Dallas, TX 75390, USA. ²Senator Paul D. Wellstone Muscular Dystrophy Cooperative Research Center, University of Texas Southwestern Medical Center, Dallas, TX 75390, USA. ³Hamon Center for Regenerative Science and Medicine, University of Texas Southwestern Medical Center, Dallas, TX 75390, USA. ⁴Department of Internal Medicine, University of Texas Southwestern Medical Center, Dallas, TX 75390, USA.

*These authors contributed equally to this work.

†Present address: Leon H. Charney Division of Cardiology, New York University School of Medicine, New York, NY 10016, USA.

‡Corresponding author. Email: Eric.Olson@UTSouthwestern.edu (E.N.O.); Chengzu.Long@nyumc.org (C.L.)

to correct this type of “hotspot” mutation, we used DMD patient fibroblast-derived induced pluripotent stem cells (iPSCs) (Riken HPS0164; abbreviated as Riken51), which harbor a deletion of exons 48 to 50, introducing a premature termination codon within exon 51 (Fig. 1A).

The splice acceptor region is generally pyrimidine-rich (26), which creates an ideal PAM sequence for genome editing by Cpf1 endonuclease (Fig. 1B). To rescue dystrophin expression in Riken51 iPSCs, we used a Cpf1 gRNA to target exon 51, introducing small insertions and deletions (INDELs) in exon 51 by NHEJ and subsequently reframing the dystrophin ORF, theoretically, in one-third of corrected genes, a process we refer to as “reframing” (Fig. 1A). We also compared two Cpf1 orthologs, LbCpf1 (from *Lachnospiraceae bacterium ND2006*) and AsCpf1 (from *Acidaminococcus sp. BV3L6*), which use the same PAM sequences for genome cleavage.

Cpf1 cleavage was targeted near the T-rich splice acceptor site of exon 51 using a gRNA (designated g1) (Fig. 1C), which was cloned into the pLbCpf1-2A-GFP and pAsCpf1-2A-GFP plasmids (Fig. 1D). These plasmids express human codon-optimized LbCpf1 or AsCpf1, plus green fluorescent protein (GFP), enabling fluorescence-activated cell sorting (FACS) of Cpf1-expressing cells (Fig. 1D). Initially, we evaluated the cleavage efficiency of Cpf1 editing with g1 in human 293T cells. Both LbCpf1 and AsCpf1 efficiently induced DNA cleavage with g1, as detected using the T7E1 assay that recognizes and cleaves nonperfectly matched DNA (Fig. 1E).

Next, we used LbCpf1 and AsCpf1 with g1 to edit Riken51 iPSCs, and using the T7E1 assay, we observed genome cleavage at *DMD* exon 51 (Fig. 1E). Genomic polymerase chain reaction (PCR) products from the Cpf1-edited *DMD* exon 51 were cloned and sequenced (fig. S1A). We observed INDELs near the exon 51 splice acceptor site in both LbCpf1- and AsCpf1-edited Riken51 iPSCs (fig. S1A). Single clones from a mixture of reframed Riken51 iPSCs were picked and expanded, and the edited genomic region was sequenced. Of the 12 clones, we observed 4 clones with reframed *DMD* exon 51, which restored the ORF (fig. S1B).

Restoration of dystrophin expression in DMD iPSC-derived cardiomyocytes after Cpf1-mediated reframing

Riken51 iPSCs edited by CRISPR-Cpf1 using the reframing strategy were induced to differentiate into cardiomyocytes (Fig. 2A) (27). Cardiomyocytes with the reframed *DMD* gene were identified by reverse transcription PCR (RT-PCR) using a forward primer targeting exon 47 and a reverse primer targeting exon 52, and the PCR products were sequenced (Fig. 2, B and C). Uncorrected iPSC-derived cardiomyocytes have a premature termination codon following the first eight amino acids encoded by exon 51 (Fig. 2C). Cardiomyocytes differentiated from Cpf1-edited Riken51 iPSCs showed restoration of the *DMD* ORF, as seen by sequencing of the RT-PCR products from amplification of exons 47 to 52 (Fig. 2C). We also confirmed restoration of dystrophin protein expression by Western blot analysis and immunocytochemistry using a dystrophin antibody (Fig. 2, D and E). Even without clonal selection and expansion, cardiomyocytes differentiated from Cpf1-edited iPSC mixtures showed levels of dystrophin protein comparable to wild-type (WT) cardiomyocytes (Fig. 2D).

From mixtures of LbCpf1-edited Riken51 iPSCs, we picked two clones (clones #2 and #5) with in-frame INDELs of different sizes and differentiated the clones into cardiomyocytes. Clone #2 had an 8-bp deletion at the 5' end of exon 51, together with an endogenous deletion of exons 48 to 50. The total 405-bp deletion restored the *DMD*

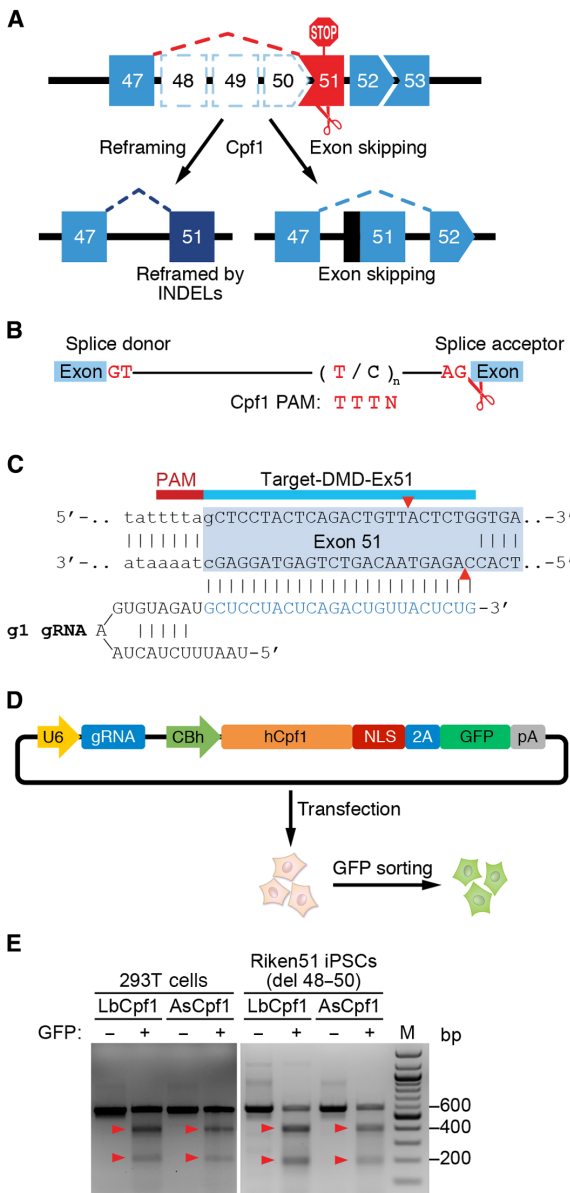


Fig. 1. Correction of DMD mutations by Cpf1-mediated genome editing. (A) A *DMD* deletion of exons 48 to 50 results in splicing of exons 47 to 51, generating an out-of-frame mutation of dystrophin. Two strategies were used for the restoration of dystrophin expression by Cpf1. In the “reframing” strategy, small INDELs in exon 51 restore the protein reading frame of dystrophin. The “exon skipping” strategy is achieved by disruption of the splice acceptor of exon 51, which results in splicing of exons 47 to 52 and restoration of the protein reading frame. (B) The 3' end of an intron is T-rich, which generates Cpf1 PAM sequences, enabling genome cleavage by Cpf1. (C) Illustration of Cpf1 gRNA targeting *DMD* exon 51. The T-rich PAM (red line) is located upstream of exon 51 near the splice acceptor site. The sequence of the Cpf1 g1 gRNA targeting exon 51 is shown, highlighting the complementary nucleotides in blue. Cpf1 cleavage produces a staggered end distal to the PAM site (demarcated by red arrowheads). The 5' region of exon 51 is shaded in light blue. Exon sequence is in uppercase letters. Intron sequence is in lowercase letters. (D) Illustration of a plasmid encoding human codon-optimized Cpf1 (hCpf1) with a nuclear localization signal (NLS) and 2A-GFP, driven by a hybrid form of cytomegalovirus and chicken β-actin promoters (CBh). The plasmid also encodes a Cpf1 gRNA driven by the U6 promoter. Cells transfected with this plasmid express GFP, allowing for selection of Cpf1-expressing cells by FACS. (E) T7E1 assays using human 293T cells or DMD iPSCs (Riken51) transfected with plasmid expressing LbCpf1 or AsCpf1, gRNA, and GFP show genome cleavage at *DMD* exon 51. Red arrowheads point to cleavage products. M, marker; bp, base pair.

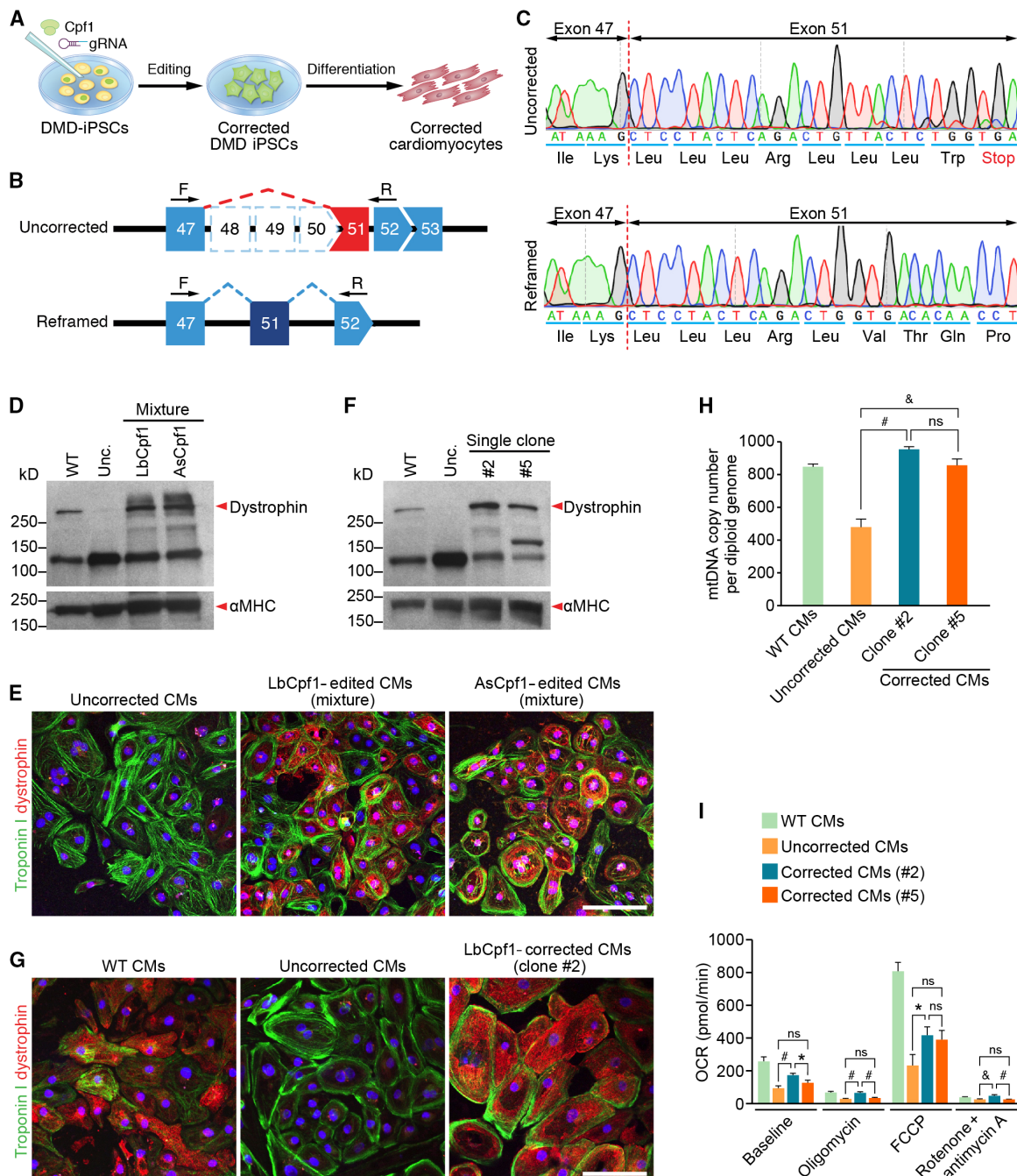


Fig. 2. DMD iPSC-derived cardiomyocytes express dystrophin after Cpf1-mediated genome editing by reframing. (A) DMD skin fibroblast-derived iPSCs were edited by Cpf1 using gRNA (corrected DMD iPSCs) and then differentiated into cardiomyocytes (corrected cardiomyocytes) for analysis of genetic correction of the *DMD* mutation. (B) A *DMD* deletion of exons 48 to 50 results in splicing of exon 47 to 51, generating an out-of-frame mutation of dystrophin. Forward primer (F) targeting exon 47 and reverse primer (R) targeting exon 52 were used in RT-PCR to confirm the reframing strategy by Cpf1-mediated genome editing in cardiomyocytes. Uncorrected cardiomyocytes lack exons 48 to 50. In contrast, after reframing, exon 51 is placed back in frame with exon 47. (C) Sequencing of representative RT-PCR products shows that uncorrected DMD iPSC-derived cardiomyocytes have a premature stop codon in exon 51, which creates a nonsense mutation. After Cpf1-mediated reframing, the ORF of dystrophin is restored. Dashed red line denotes exon boundary. (D) Western blot analysis shows dystrophin expression in a mixture of DMD iPSC-derived cardiomyocytes edited by reframing with LbCpf1 or AsCpf1 and g1 gRNA. Even without clonal selection, Cpf1-mediated reframing is efficient and sufficient to restore dystrophin expression in the cardiomyocyte mixture. α -Myosin heavy chain (α MHC) is loading control. (E) Immunocytochemistry shows dystrophin expression in iPSC-derived cardiomyocyte (CM) mixtures following LbCpf1- or AsCpf1-mediated reframing. Red, dystrophin staining; green, troponin I staining. Scale bar, 100 μ m. (F) Western blot analysis shows dystrophin expression in single clones (#2 and #5) of iPSC-derived cardiomyocytes following clonal selection after LbCpf1-mediated reframing. α MHC is loading control. (G) Immunocytochemistry shows dystrophin expression in clone #2 LbCpf1-edited iPSC-derived cardiomyocytes. Scale bar, 100 μ m. (H) Quantification of mtDNA copy number in single clones (#2 and #5) of LbCpf1-edited iPSC-derived cardiomyocytes. Data are means \pm SEM (n = 3). *P < 0.05 and #P < 0.005. ns, not significant. (I) Basal OCR of single clones (#2 and #5) of LbCpf1-edited iPSC-derived cardiomyocytes, and OCR in response to oligomycin, FCCP, rotenone, and antimycin A, normalized to cell number. Data are means \pm SEM (n = 5). *P < 0.05, &P < 0.01, and #P < 0.005.

ORF and allowed for the production of a truncated dystrophin protein with a 135-amino acid deletion. Clone #5 had a 17-bp deletion in exon 51 and produced dystrophin protein with a 138-amino acid deletion. Although there is high efficiency of cleavage by Cpf1, the amount of DNA inserted or deleted at the cleavage site varies. Additionally, INDELs can generate extra codons at the edited locus, causing changes of the ORF. The dystrophin protein expressed by clone #2 cardiomyocytes generated an additional four amino acids (Leu-Leu-Leu-Arg) between exon 47 and exon 51, whereas dystrophin protein expressed by clone #5 cardiomyocytes generated only one additional amino acid (Leu). From both clones #2 and #5, we observed restored dystrophin protein by Western blot analysis and immunocytochemistry (Fig. 2, F and G). Because of the large size of dystrophin, the internally deleted forms migrated similarly to WT dystrophin on SDS-polyacrylamide gel electrophoresis.

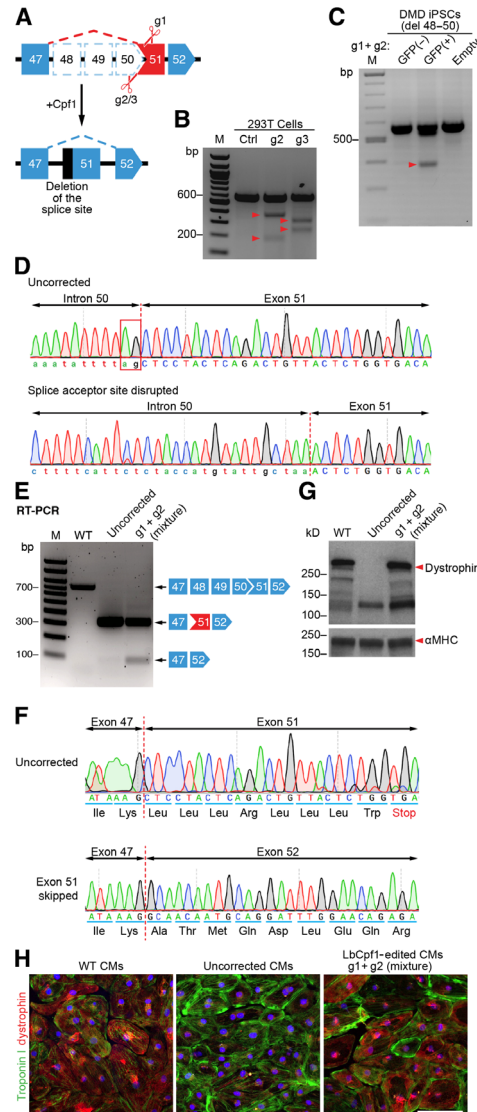
We also performed functional analysis of DMD iPSC-derived cardiomyocytes by measuring mitochondrial DNA (mtDNA) copy number and cellular respiration rates. Uncorrected DMD iPSC-derived cardiomyocytes had significantly fewer mitochondria than the LbCpf1-corrected cardiomyocytes (Fig. 2H). After LbCpf1-mediated reframing, both corrected clones restored mitochondrial number to a level comparable to that of WT cardiomyocytes (Fig. 2H). Clone #2 iPSC-derived cardiomyocytes also showed an increase in oxygen consumption rate (OCR) compared to uncorrected iPSC-derived cardiomyocytes at baseline (Fig. 2I). OCR was inhibited by oligomycin in all iPSC-derived cardiomyocytes, and treatment with the uncoupling agent FCCP (carbonyl cyanide *p*-trifluoromethoxyphenylhydrazone) enhanced OCR. Finally, treatment with rotenone and antimycin A further inhibited OCR in all cardiomyocytes. These results demonstrate that Cpf1-mediated *DMD* correction improved respiratory capacity of mitochondria in corrected iPSC-derived cardiomyocytes. Our findings show that Cpf1-mediated reframing is a highly efficient strategy to rescue DMD phenotypes in human cardiomyocytes.

Restoration of dystrophin expression in DMD iPSC-derived cardiomyocytes by Cpf1-mediated exon skipping

In contrast to the single gRNA-mediated reframing method, which introduces small INDELs, exon skipping uses two gRNAs to disrupt splice sites and generates a large deletion (Fig. 3A). As an independent strategy to restore dystrophin expression in the Riken51 iPSCs, we designed two LbCpf1 gRNAs (g2 and g3) that target the 3' end of intron 50 and tested the cleavage efficiency in human 293T cells. The T7E1 assay showed that g2 had higher cleavage efficiency within intron 50 compared to g3 (Fig. 3B). Therefore, we co-delivered LbCpf1, g2, and g1 (g1 targets the 5' region of exon 51) into Riken51 iPSCs, with the aim of disrupting the splice acceptor site of exon 51. Genomic PCR showed a lower band in LbCpf1-edited iPSCs (Fig. 3C), and sequencing data confirmed the presence of a deletion of ~200 bp between intron 50 and exon 51, which disrupted the conserved splice acceptor site (Fig. 3D).

Targeting specificity of Cpf1 was evaluated using the top 10 potential genome-wide off-target sites (OT-01 to OT-10) for each gRNA, as predicted by Cas-OFFinder (www.rgenome.net/cas-offinder/) (tables S1 and S2). Efficient cleavage bands were observed at the on-target site, and most of the off-target sites did not show a detectable cleavage band by the T7E1 assay (fig. S2) or by quantitative capillary electrophoresis using a fragment analyzer (figs. S3 and S4).

Riken51 iPSCs edited by the exon skipping strategy with g1 and g2 were differentiated into cardiomyocytes. Cells harboring the edited *DMD* allele were identified by RT-PCR using a forward primer targeting exon 47 and a reverse primer targeting exon 52, showing deletion of the exon



51 splice acceptor site, which allows skipping of exon 51 (Fig. 3E). Sequencing of the RT-PCR products confirmed that exon 47 was spliced to exon 52, which restored the *DMD* ORF (Fig. 3F). Western blot analysis and immunocytochemistry confirmed the restoration of dystrophin protein expression in a mixture of LbCpf1-edited cardiomyocytes with g1 and g2 (Fig. 3, G and H). Thus, Cpf1 editing by the exon skipping strategy is highly efficient in rescuing the DMD phenotype in human cardiomyocytes.

Restoration of dystrophin in *mdx* mice by Cpf1-mediated correction

To further evaluate the potential of Cpf1-mediated *Dmd* correction in vivo, we used LbCpf1 to permanently correct the mutation in the germ line of *mdx* mice by HDR-mediated correction or NHEJ-mediated re-framing. *mdx* mice carry a nonsense mutation in exon 23 of the *Dmd* gene because of a C-to-T transition (Fig. 4A). Three gRNAs (g1, g2, and g3) that target exon 23 were screened and tested in mouse 10T1/2 fibroblasts for cleavage efficiency (Fig. 4B). The T7E1 assay revealed that LbCpf1 and AsCpf1 had different cleavage efficiencies at *Dmd* exon 23 (Fig. 4C). On the basis of sequencing results, LbCpf1-mediated genome editing using g2 generated a greater occurrence of INDELs in mouse fibroblasts compared to g3 (fig. S1C).

LbCpf1 editing with g2 recognizes a PAM sequence 9 bp upstream of the mutation site and creates a staggered double-stranded DNA cut 8 bp downstream of the mutation site (Fig. 4D). To obtain HDR genome editing, we used a 180-bp single-stranded oligodeoxynucleotide (ssODN) in combination with LbCpf1 and g2, because it has been shown that ssODNs are more efficient in introducing small genomic modifications than double-stranded donor plasmids (6, 7). We generated an ssODN containing 90 bp of sequence homology flanking the cleavage site, including four silent mutations and a Tse I restriction site to facilitate genotyping, as previously described (7). This ssODN was designed to be used with LbCpf1 and g2 to correct the C-to-T mutation within *Dmd* exon 23 and to restore dystrophin in *mdx* mice by HDR.

Correction of muscular dystrophy in *mdx* mice by LbCpf1-mediated HDR or NHEJ

mdx zygotes were coinjected with in vitro transcribed LbCpf1 mRNA, in vitro transcribed g2 gRNA, and 180-bp ssODN and reimplanted into pseudopregnant females (Fig. 5A). Three litters of LbCpf1-edited *mdx* mice were analyzed by the T7E1 assay and Tse I RFLP (restriction fragment length polymorphism) (Fig. 5, B and C). Of the 24 pups born, 12 were T7E1-positive and 5 carried corrected alleles (*mdx*-C1 to *mdx*-C5), as detected by Tse I RFLP and sequencing (Fig. 5, C and D). Skeletal muscles (tibialis anterior and gastrocnemius/plantaris) from WT, *mdx*, and LbCpf1-corrected *mdx*-C mice were analyzed at 4 weeks of age. Hematoxylin and eosin (H&E) staining of muscle showed fibrosis and inflammatory infiltration in *mdx* muscle, whereas LbCpf1-corrected (*mdx*-C) muscle displayed normal muscle morphology and no signs of a dystrophic phenotype (Fig. 5E and fig. S5, A and B). Immunohistochemistry showed the absence of dystrophin-positive fibers in muscle sections of *mdx* mice, whereas *mdx*-C muscle corrected by LbCpf1-mediated HDR showed dystrophin protein expression in a majority of muscle fibers (Fig. 5F and fig. S5, A and B).

Additionally, we performed histological analysis of different tissues from multiple *mdx*-C mice with correction rates from 8 to 50%. All LbCpf1-corrected *mdx*-C mice showed restored dystrophin expression in multiple tissues, including skeletal muscles, heart, and brain (figs. S6 and S7). Muscle of *mdx*-C mice with 50% genomic correction showed

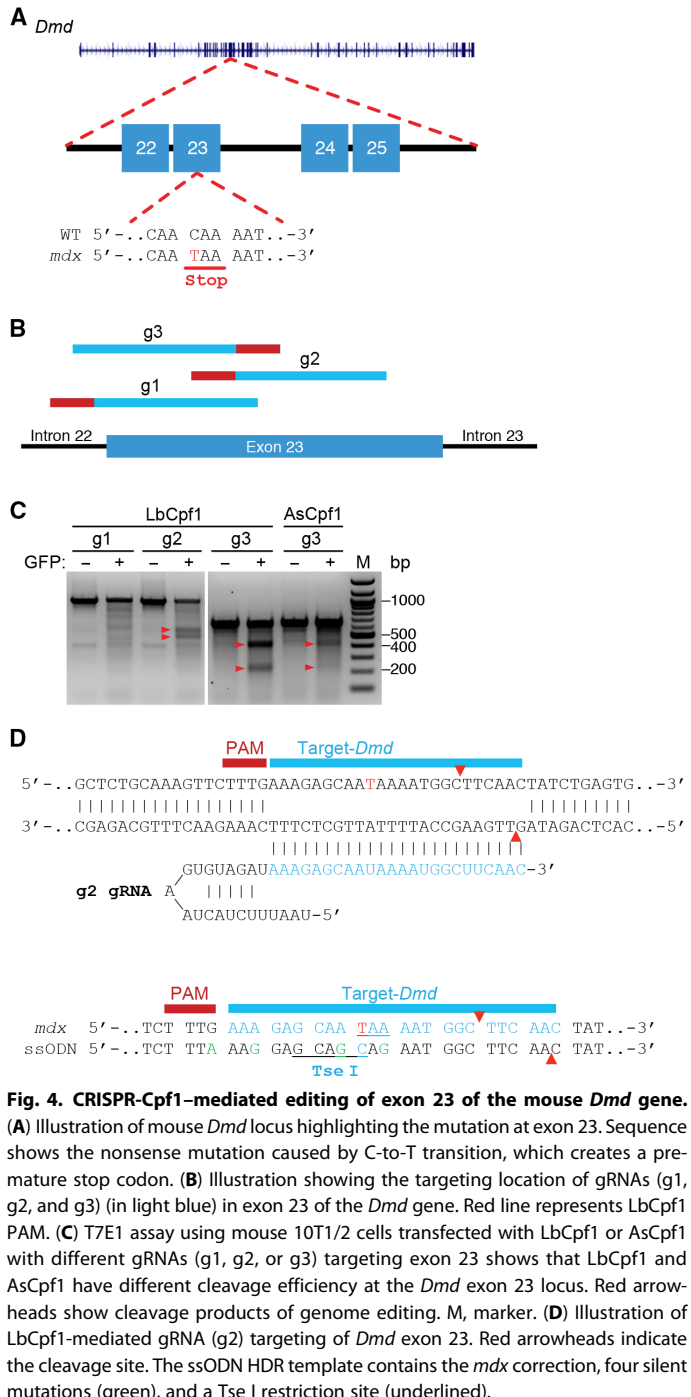


Fig. 4. CRISPR-Cpf1-mediated editing of exon 23 of the mouse *Dmd* gene. (A) Illustration of mouse *Dmd* locus highlighting the mutation at exon 23. Sequence shows the nonsense mutation caused by C-to-T transition, which creates a premature stop codon. (B) Illustration showing the targeting location of gRNAs (g1, g2, and g3) (in light blue) in exon 23 of the *Dmd* gene. Red line represents LbCpf1 PAM. (C) T7E1 assay using mouse 10T1/2 cells transfected with LbCpf1 or AsCpf1 with different gRNAs (g1, g2, or g3) targeting exon 23 shows that LbCpf1 and AsCpf1 have different cleavage efficiency at the *Dmd* exon 23 locus. Red arrowheads show cleavage products of genome editing. M, marker. (D) Illustration of LbCpf1-mediated gRNA (g2) targeting of *Dmd* exon 23. Red arrowheads indicate the cleavage site. The ssODN HDR template contains the *mdx* correction, four silent mutations (green), and a Tse I restriction site (underlined).

full restoration of dystrophin protein and displayed no sign of fibrosis or inflammatory infiltration, which is consistent with our previous study (7). Western blot analysis showed expression of dystrophin protein in multiple skeletal muscle groups, heart, and brain (fig. S8), consistent with percentages of dystrophin-positive fibers seen with immunohistochemistry (fig. S6).

LbCpf1-mediated correction of the *Dmd* mutation in germ cells was evaluated in eggs and sperm of LbCpf1-corrected *mdx*-C mice by T7E1 assays and Tse I RFLP. All LbCpf1-corrected *mdx*-C mice carried a corrected allele in their germ cells (fig. S9). Genome editing efficiency

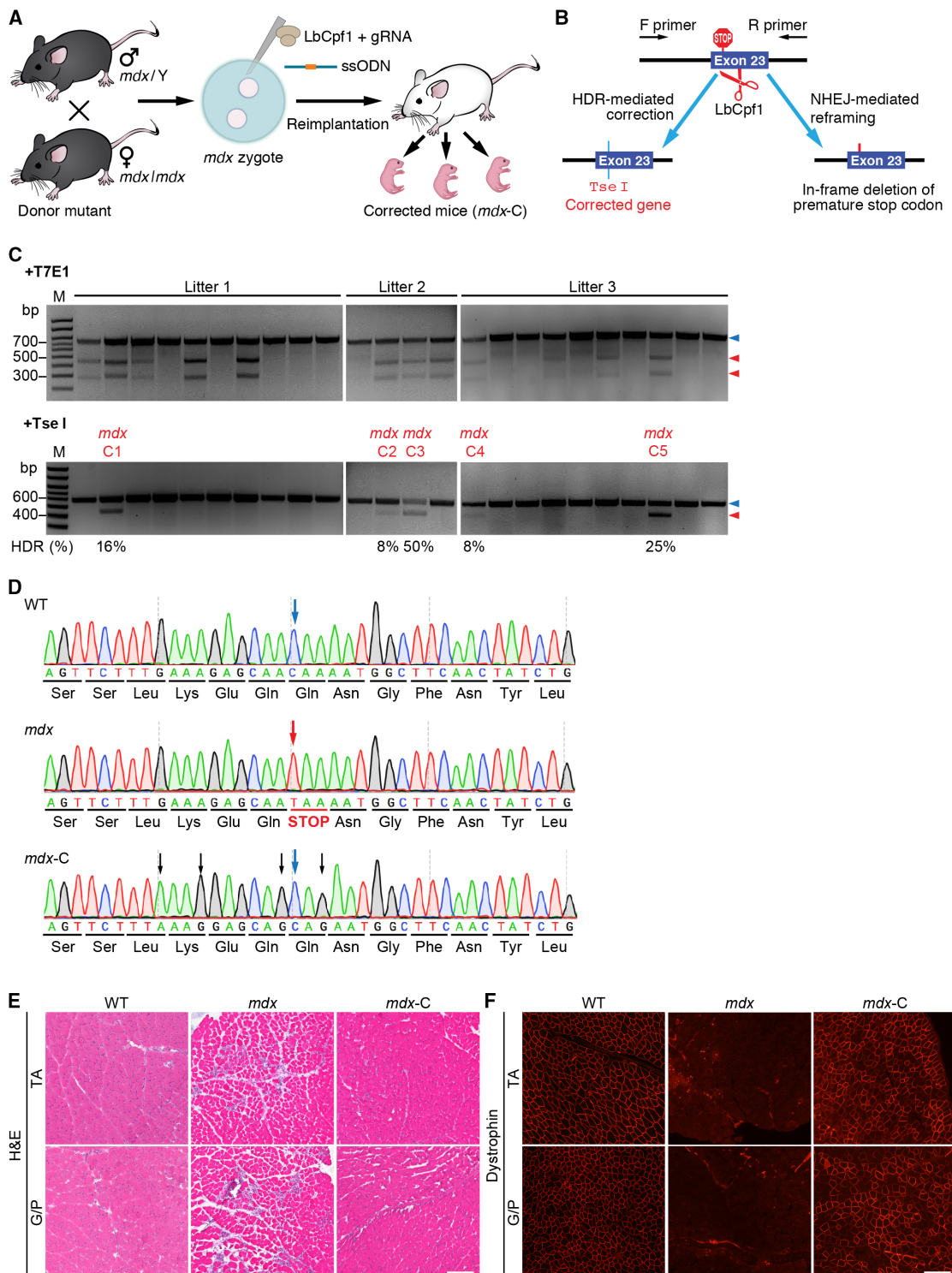


Fig. 5. CRISPR-LbCpf1-mediated *Dmd* correction in *mdx* mice. (A) Strategy of gene correction in *mdx* mice by LbCpf1-mediated germline editing. Zygotes from intercrosses of *mdx* parents were injected with gene editing components (LbCpf1 mRNA, g2 gRNA, and ssODN) and reimplanted into pseudopregnant mothers, which gave rise to pups with gene correction (*mdx*-C). (B) Illustration showing LbCpf1 correction of *mdx* allele by HDR or NHEJ. (C) Genotyping results of LbCpf1-edited *mdx* mice. Top: T7E1 assay. Blue arrowhead denotes uncleaved DNA, and red arrowhead shows T7E1-cleaved DNA. Bottom: Tse I RFLP assay. Blue arrowhead denotes uncorrected DNA, and red arrowhead points to Tse I cleavage, indicating HDR correction. *mdx*-C1 to *mdx*-C5 denote LbCpf1-edited *mdx* mice. (D) Top: Sequence of WT *Dmd* exon 23. Middle: Sequence of *mdx* *Dmd* exon 23 with C-to-T mutation, which generates a stop codon. Bottom: Sequence of *Dmd* exon 23 with HDR correction by LbCpf1-mediated editing. Black arrows point to silent mutations introduced by the ssODN HDR template. (E) H&E staining of tibialis anterior (TA) and gastrocnemius/plantaris (G/P) muscles from WT, *mdx*, and LbCpf1-edited mice (*mdx*-C). Scale bar, 100 μm. (F) Immunohistochemistry of tibialis anterior and gastrocnemius/plantaris muscles from WT, *mdx*, and LbCpf1-edited mice (*mdx*-C) using an antibody to dystrophin (red). *mdx* muscle showed fibrosis and inflammatory infiltration, whereas *mdx*-C muscle showed normal muscle structure.

Table 1. Serum CK measurement and forelimb grip strength of WT, *mdx*, and LbCpf1-corrected *mdx*-C mice. M, male; F, female.

Mouse no.	Percent correction by HDR	Sex	Weight (g)	CK (U/liter)	Forelimb grip strength (grams of force)						Average ± SD
					Trial 1	Trial 2	Trial 3	Trial 4	Trial 5	Trial 6	
WT-1	—	M	16.6	455	103	106	97	71	88	82	91.2 ± 13.4
WT-2	—	M	19.5	220	87	95	73	73	74	78	80.0 ± 9.1
WT-3	—	M	18.7	306	79	97	74	78	84	84	82.7 ± 8.0
WT-4	—	F	15.5	184	86	97	85	83	85	88	87.3 ± 5.0
WT-5	—	F	15.4	175	88	85	100	96	88	86	90.5 ± 6.1
WT-6	—	F	12.6	157	76	75	73	78	64	61	71.2 ± 7.0
<i>mdx</i> -1	0	M	18.8	8579	76	92	86	33	32	29	58.0 ± 29.9
<i>mdx</i> -2	0	M	21.0	9440	62	58	54	45	45	47	51.8 ± 7.3
<i>mdx</i> -3	0	M	21.5	5936	77	54	69	57	56	61	62.3 ± 8.9
<i>mdx</i> -4	0	F	16.1	6306	69	63	69	61	67	60	64.8 ± 4.0
<i>mdx</i> -5	0	F	15.8	6349	83	88	85	59	55	54	70.7 ± 16.2
<i>mdx</i> -6	0	F	16.2	4168	69	71	53	59	59	57	61.3 ± 7.1
<i>mdx</i> -C1	16%	F	21.7	1233	112	111	112	115	101	109	110.0 ± 4.8
<i>mdx</i> -C2	8%	F	19.7	4920	119	109	108	95	86	85	100.3 ± 13.8
<i>mdx</i> -C3	50%	F	20.2	248	110	115	114	112	112	104	111.2 ± 3.9
<i>mdx</i> -C4	8%	M	22.7	6607	49	45	42	30	25	21	35.3 ± 11.5
<i>mdx</i> -C5	25%	F	17.7	3239	92	110	96	91	110	95	99.0 ± 8.7

of Cas9 and LbCpf1 was compared at the *Dmd* exon 23 locus, and no significant difference was observed (table S3).

Physiological and functional analyses were also performed in WT, *mdx*, and LbCpf1-corrected *mdx*-C mice. Serum creatine kinase (CK) levels were decreased substantially in *mdx*-C mice and were inversely correlated with the percentage of genome correction (Table 1). The forelimb grip strength test indicated that LbCpf1-corrected *mdx*-C mice had improved muscle strength compared to *mdx* mice (Table 1).

DISCUSSION

Here, we show that the newly discovered CRISPR-Cpf1 nuclease can efficiently correct *DMD* mutations in patient-derived iPSCs and *mdx* mice, allowing for restoration of dystrophin expression. Lack of dystrophin in DMD has been shown to disrupt the integrity of the sarcolemma, causing mitochondrial dysfunction and oxidative stress (28, 29). We found increased mtDNA and higher OCRs in LbCpf1-corrected iPSC-derived cardiomyocytes compared to uncorrected DMD iPSC-derived cardiomyocytes. Metabolic abnormalities of human DMD iPSC-derived cardiomyocytes were also rescued by Cpf1-mediated genomic editing. Our findings also demonstrated the robustness and efficiency of Cpf1 in mouse genome editing. By using HDR-mediated correction, the ORF of the mouse *Dmd* gene was completely restored, and pathophysiological hallmarks of the dystrophic phenotype, such as fibrosis and inflammatory infiltration, were also rescued.

Two different strategies—reframing and exon skipping—were applied to restore the ORF of the *DMD* gene using LbCpf1-mediated genome editing. Reframing creates small INDELS and restores the ORF by placing out-of-frame codons in frame. Only one gRNA is required for reframing. Although we did not observe any differences in subcellular localization between WT dystrophin protein and reframed dystrophin protein by immunocytochemistry, we observed differences in dystrophin expression level, mtDNA quantity, and OCR in different edited clones, suggesting that reframed dystrophin may not be structurally or functionally identical to WT dystrophin.

Various issues should be considered with respect to the use of one or two gRNAs with Cpf1 editing. Here, we show that two gRNAs are more effective than one gRNA for disruption of the splice acceptor site compared to reframing. When using two gRNAs, Cpf1 editing excises the intervening region and not only removes the splice acceptor site but also can be designed to remove deleterious “AG” nucleotides, eliminating the possibility of generating a pseudosplice acceptor site. However, with two gRNAs, there is the necessity that both gRNAs cleave simultaneously, which may not occur. If only one of the two gRNAs cleaves, the desired deletion will not be generated. However, there remains the possibility that cleavage with one of the two gRNAs will generate INDELS at the targeted exon region, reframing the ORF, because in theory, one-third of the INDELS will be in frame. Using one gRNA to disrupt the splice acceptor site seems more efficient because it eliminates the need for two simultaneous cuts to occur. However, there is uncertainty with respect to the length of the INDEL generated by one gRNA-mediated

editing. With one gRNA, there remains the possibility of leaving exonic AG nucleotides near the cleavage site, which can serve as an alternative pseudosplice acceptor site.

With its unique T-rich PAM sequence, Cpf1 further expands the genome editing range of the CRISPR family, which is important for potential correction of other disease-related mutations because not all mutation sites contain G-rich PAM sequences for SpCas9 or PAMs for other Cas9 orthologs. Moreover, the staggered cut generated by Cpf1 may also be advantageous for NHEJ-mediated genome editing (30). Finally, the LbCpf1 used in this study is 140 amino acids smaller than the most widely used SpCas9, which would enhance packaging and delivery by AAV.

Our off-target analysis by T7E1 assays and quantitative capillary electrophoresis using a fragment analyzer showed similar results to previous reports (16, 17), indicating that LbCpf1 and AsCpf1 had high genome-wide targeting efficiency and high specificity comparable to those of SpCas9. This is reflective of LbCpf1 and AsCpf1 not tolerating mismatches at the 5' PAM proximal region, thereby lessening the frequency of off-targeting effect.

Our findings show that Cpf1 is highly efficient in correcting human *DMD* and mouse *Dmd* mutations in vitro and in vivo. CRISPR-Cpf1–mediated genome editing represents a new and powerful approach to permanently eliminate genetic mutations and rescue abnormalities associated with DMD and other disorders.

MATERIALS AND METHODS

Generation of pLbCpf1-2A-GFP and pAsCpf1-2A-GFP plasmids

Human codon-optimized LbCpf1 and AsCpf1 were PCR-amplified from the pY016 plasmid (14) (pcDNA3.1-hLbCpf1), a gift from F. Zhang (Addgene plasmid #69988), and the pY010 plasmid (14) (pcDNA3.1-hAsCpf1), a gift from F. Zhang (Addgene plasmid #69982), respectively. Cpf1 complementary DNA (cDNA) and 2A-GFP DNA fragment were cloned into the backbone of the pSpCas9(BB)-2A-GFP (PX458) plasmid (13), a gift from F. Zhang (Addgene plasmid #48138), which was cut with Age I/Eco RI to remove SpCas9(BB)-2A-GFP. In-Fusion HD Cloning Kit (Takara Bio) was used. Cpf1 gRNAs targeting the human *DMD* or the mouse *Dmd* locus were subcloned into newly generated pLbCpf1-2A-GFP and pAsCpf1-2A-GFP plasmids using Bbs I digestion and T4 ligation. Detailed primer sequences can be found in the Supplementary Materials (table S4).

Human iPSC maintenance, nucleofection, and differentiation

Human iPSCs (RBRC-HPS0164) were purchased from Cell Bank RIKEN BioResource Center. Human iPSCs were cultured in mTeSR1 medium (STEMCELL Technologies) and passaged approximately every 4 days (1:18 split ratio). One hour before nucleofection, iPSCs were treated with 10 μM ROCK inhibitor (Y-27632) and dissociated into single cells using Accutase (Innovative Cell Technologies Inc.). iPSCs (1×10^6) were mixed with 5 μg of the pLbCpf1-2A-GFP or pAsCpf1-2A-GFP plasmid and nucleofected using the P3 Primary Cell 4D-Nucleofector X Kit (Lonza) according to the manufacturer's protocol. After nucleofection, iPSCs were cultured in mTeSR1 medium supplemented with 10 μM ROCK inhibitor, penicillin-streptomycin (1:100) (Thermo Fisher Scientific), and Primocin (100 μg/ml; InvivoGen). Three days after nucleofection, GFP(+) and GFP(−) cells were sorted by FACS and subjected to the T7E1 assay. Single clones derived from GFP(+) iPSCs

were picked and sequenced. iPSCs were induced to differentiate into cardiomyocytes, as previously described (27).

Genomic DNA isolation

Genomic DNA of mouse 10T1/2 fibroblasts and human iPSCs was isolated using a Quick-gDNA MiniPrep kit (Zymo Research) according to the manufacturer's protocol.

Reverse transcription PCR

RNA was isolated using TRIzol (Thermo Fisher Scientific) according to the manufacturer's protocol. cDNA was synthesized using the iScript Reverse Transcription Supermix (Bio-Rad Laboratories) according to the manufacturer's protocol. RT-PCR was performed using primers flanking *DMD* exons 47 and 52 (forward, 5'-CCCAGAAGAGCAA-GATAAACTTGAA-3'; reverse, 5'-CTCTGTTCCAAATCCTGC-TTGT-3'). RT-PCR products amplified from WT cardiomyocytes, uncorrected cardiomyocytes, and exon 51-skipped cardiomyocytes were 712, 320, and 87 bp, respectively.

Dystrophin Western blot analysis

Western blot analysis for human iPSC-derived cardiomyocytes was performed, as previously described (7), using a rabbit anti-dystrophin antibody (Abcam, ab15277) and a mouse anti-cardiac myosin heavy chain antibody (Abcam, ab50967). For mouse skeletal muscles, heart, and brain, the Western blot was performed, as previously described (7), using a mouse anti-dystrophin antibody (Sigma-Aldrich, D8168) and a mouse anti-vinculin antibody (Sigma-Aldrich, V9131).

Dystrophin immunocytochemistry and immunohistochemistry

iPSC-derived cardiomyocytes were fixed with acetone, blocked with serum cocktail [2% normal horse serum/2% normal donkey serum/0.2% bovine serum albumin (BSA)/phosphate-buffered saline (PBS)], and incubated with a dystrophin antibody (MANDYS8, 1:800; Sigma-Aldrich) and troponin I antibody (H170, 1:200; Santa Cruz Biotechnology) in 0.2% BSA/PBS. Following overnight incubation at 4°C, they were incubated with secondary antibodies [biotinylated horse anti-mouse immunoglobulin G (IgG), 1:200 (Vector Laboratories), and fluorescein-conjugated donkey anti-rabbit IgG, 1:50 (Jackson ImmunoResearch)] for 1 hour. Nuclei were counterstained with Hoechst 33342 (Molecular Probes).

Immunohistochemistry of skeletal muscles, heart, and brain was performed, as previously described (7, 12), using a dystrophin antibody (MANDYS8, 1:800; Sigma-Aldrich). Nuclei were counterstained with Hoechst 33342 (Molecular Probes).

mtDNA copy number quantification

Genomic DNA and mtDNA were isolated using TRIzol, followed by back extraction, as previously described (31). KAPA SYBR FAST qPCR Kit (Kapa Biosystems) was used to perform real-time PCR to quantitatively determine mtDNA copy number. Human mitochondrial *ND1* gene was amplified using primers (forward, 5'-CGCACATCTAC-CATCACCCCTC-3'; reverse, 5'-CGGCTAGGCTAGAGGTGGCTA-3'). Human genomic *LPL* gene was amplified using primers (forward, 5'-GAGTATGCAGAACGCCCGAGTC-3'; reverse, 5'-TCAA-CATGCCCAACTGGTTCTGG-3'). mtDNA copy number per diploid genome was calculated using the following formulas: $\Delta C_T = (\text{mtND1 } C_T - \text{LPL } C_T)$ and mtDNA copy number per diploid genome = $2 \times 2^{-\Delta C_T}$.

Cellular respiration rates

OCRs were determined in human iPSC-derived cardiomyocytes using the XF24 Extracellular Flux Analyzer (Seahorse Bioscience) following the manufacturer's protocol, as previously described (32).

In vitro transcription of LbCpf1 mRNA and gRNA

Human codon-optimized LbCpf1 was PCR-amplified from pLbCpf1-2A-GFP to include the T7 promoter sequence (table S4). The PCR product was transcribed using the mMESSAGE mMACHINE T7 Transcription Kit (Thermo Fisher Scientific) according to the manufacturer's protocol. Synthesized LbCpf1 mRNAs were polyadenylate [poly(A)]-tailed with *E. coli* Poly(A) Polymerase (New England Biolabs) and purified using NucAway spin columns (Thermo Fisher Scientific).

The template for LbCpf1 gRNA in vitro transcription was PCR-amplified from the pLbCpf1-2A-GFP plasmid and purified using the Wizard SV Gel and PCR Clean-Up System (Promega). The LbCpf1 gRNA was synthesized using the MEGAshortscript T7 Transcription Kit (Thermo Fisher Scientific) according to the manufacturer's protocol. Synthesized LbCpf1 gRNA was purified using NucAway spin columns (Thermo Fisher Scientific).

Single-stranded oligodeoxynucleotide

ssODN was used as HDR template and synthesized by Integrated DNA Technologies as 4 nM Ultramer oligonucleotides. ssODN was mixed with LbCpf1 mRNA and gRNA directly without purification. The sequence of ssODN is as follows: 5'-TGATATGAATGAACTCAT-CAAATATGCGTGTAGTGTAAATGAACCTCTATTAACTT-GAGGCTCTGAAAGTTCTTAAAGGAGCAGCAGAATGGCTT-CAACTATCTGAGTGAACACTGTGAAGGAGATGGCCAAGAAAG-CACCTTCAGAAATATGCCAGAAATCTGTCAGAATT-3'.

CRISPR-Cpf1-mediated genome editing by one-cell embryo injection

All animal procedures were approved by the Institutional Animal Care and Use Committee at the University of Texas Southwestern Medical Center. Detailed injection procedures were performed as described previously (7). The only modification was replacing Cas9 mRNA and Cas9 gRNAs with LbCpf1 mRNA and LbCpf1 gRNAs, respectively.

PCR amplification of genomic DNA, T7E1 assay, and Tse I RFLP analysis

All these protocols were preformed as previously published (7).

Mouse forelimb grip strength test and serum CK measurement

Grip strength test and serum CK measurement were performed, as previously described (7), by the Neuro-Models Core Facility and the Metabolic Phenotyping Core at the University of Texas Southwestern Medical Center, respectively.

Off-target site analysis

Off-target sites were predicted using Cas-OFFinder (www.rgenome.net/cas-offinder/), and off-target analysis was performed as previously described (12). Sequences are provided in the Supplementary Materials (tables S1 and S2). For capillary electrophoresis, PCR products from control and treated samples were denatured and reannealed to form heteroduplex. T7E1-digested DNA samples were visualized by the Fragment Analyzer (Advanced Analytical), which allowed a sensitive, accurate, and fast quantification of percent cleavage. The PCR sample (2 μl)

was diluted with the sample buffer (DNF-910-1000CP CRISPR kit) and loaded into the 96-well sample plate. Cleavage percentage was calculated by CRISPR Plugin for PROSize 2.0. Expected full-length and cleavage fragment sizes of PCR samples were entered into the software. Highlighted fragments with automated scores were shown in figs. S3B and S4B. Concentration of each peak and percentage cleavage value were automatically calculated by the software. Reconstructed gel images from the Fragment Analyzer electropherogram were shown in figs. S3A and S4A.

Statistical analysis

Statistical analysis was assessed by two-tailed Student's *t* test. Data are shown as means ± SEM. A *P* < 0.05 value was considered statistically significant.

SUPPLEMENTARY MATERIALS

Supplementary material for this article is available at <http://advances.sciencemag.org/cgi/content/full/3/4/e1602814/DC1>

fig. S1. Genome editing of *DMD* exon 51 and *Dmd* exon 23 by LbCpf1 or AsCpf1.

fig. S2. Genomic PCR and T7E1 assay of off-target sites.

fig. S3. Capillary electrophoresis and fragment analysis of *DMD* g1 off-target sites.

fig. S4. Capillary electrophoresis and fragment analysis of *DMD* g2 off-target sites.

fig. S5. Histological analysis of muscles from WT, *mdx*, and LbCpf1-edited mice (*mdx*-C).

fig. S6. Immunohistochemistry of skeletal muscles, heart, and brain from WT, *mdx*, and LbCpf1-edited mice (*mdx*-C).

fig. S7. H&E staining of skeletal muscles, heart, and brain from WT, *mdx*, and LbCpf1-edited mice (*mdx*-C).

fig. S8. Western blot analysis of skeletal muscles, heart, and brain from WT, *mdx*, and LbCpf1-edited mice (*mdx*-C).

fig. S9. T7E1 and Tse I RFLP analysis of germ cells from LbCpf1-edited mice (*mdx*-C) and uncorrected *mdx* mice.

table S1. Sequence of the on-target site and 10 potential off-target sites.

table S2. Primers used in the off-target site analysis.

table S3. Comparison of CRISPR-Cas9- and CRISPR-Cpf1-mediated HDR correction in *mdx* mice.

table S4. Sequence of primers.

REFERENCES AND NOTES

1. K. P. Campbell, S. D. Kahl, Association of dystrophin and an integral membrane glycoprotein. *Nature* **338**, 259–262 (1989).
2. K. Hollinger, J. S. Chamberlain, Viral vector-mediated gene therapies. *Curr. Opin. Neurol.* **28**, 522–527 (2015).
3. B. Bostick, J.-H. Shin, Y. Yue, D. Duan, AAV-microdystrophin therapy improves cardiac performance in aged female *mdx* mice. *Mol. Ther.* **19**, 1826–1832 (2011).
4. Y. Shimizu-Motohashi, S. Miyatake, H. Komaki, S. Takeda, Y. Aoki, Recent advances in innovative therapeutic approaches for Duchenne muscular dystrophy: From discovery to clinical trials. *Am. J. Transl. Res.* **8**, 2471–2489 (2016).
5. F. J. M. Mojica, C. Díez-Villaseñor, J. García-Martínez, E. Soria, Intervening sequences of regularly spaced prokaryotic repeats derive from foreign genetic elements. *J. Mol. Evol.* **60**, 174–182 (2005).
6. Y. Wu, D. Liang, Y. Wang, M. Bai, W. Tang, S. Bao, Z. Yan, D. Li, J. Li, Correction of a genetic disease in mouse via use of CRISPR-Cas9. *Cell Stem Cell* **13**, 659–662 (2013).
7. C. Long, J. R. McAnally, J. M. Shelton, A. A. Mireault, R. Bassel-Duby, E. N. Olson, Prevention of muscular dystrophy in mice by CRISPR/Cas9-mediated editing of germline DNA. *Science* **345**, 1184–1188 (2014).
8. H. Yin, W. Xue, S. Chen, R. L. Bogorad, E. Benedetti, M. Grompe, V. Koteliansky, P. A. Sharp, T. Jacks, D. G. Anderson, Genome editing with Cas9 in adult mice corrects a disease mutation and phenotype. *Nat. Biotechnol.* **32**, 551–553 (2014).
9. M. Tabebordbar, K. Zhu, J. K. W. Cheng, W. L. Chew, J. J. Widrick, W. X. Yan, C. Maesner, E. Y. Wu, R. Xiao, F. A. Ran, L. Cong, F. Zhang, L. H. Vandenberghe, G. M. Church, A. J. Wagers, In vivo gene editing in dystrophic mouse muscle and muscle stem cells. *Science* **351**, 407–411 (2016).
10. C. E. Nelson, C. H. Hakim, D. G. Ousterout, P. I. Thakore, E. A. Moreb, R. M. Castellanos Rivera, S. Madhavan, X. Pan, F. A. Ran, W. X. Yan, A. Asokan, F. Zhang, D. Duan, C. A. Gersbach, In vivo genome editing improves muscle function in a mouse model of Duchenne muscular dystrophy. *Science* **351**, 403–407 (2016).

11. M. A. DeWitt, W. Magis, N. L. Bray, T. Wang, J. R. Berman, F. Urbinati, S.-J. Heo, T. Mitros, D. P. Muñoz, D. Boffelli, D. B. Kohn, M. C. Walters, D. Carroll, D. I. K. Martin, J. E. Corn, Selection-free genome editing of the sickle mutation in human adult hematopoietic stem/progenitor cells. *Sci. Transl. Med.* **8**, 360ra134 (2016).
12. C. Long, L. Amoasii, R. Bassel-Duby, E. N. Olson, Genome editing of monogenic neuromuscular diseases: A systematic review. *JAMA Neurol.* **73**, 1349–1355 (2016).
13. F. A. Ran, L. Cong, W. X. Yan, D. A. Scott, J. S. Gootenberg, A. J. Kriz, B. Zetsche, O. Shalem, X. Wu, K. S. Makarova, E. V. Koonin, P. A. Sharp, F. Zhang, In vivo genome editing using *Staphylococcus aureus* Cas9. *Nature* **520**, 186–191 (2015).
14. B. Zetsche, J. S. Gootenberg, O. O. Abudayyeh, I. M. Slaymaker, K. S. Makarova, P. Essletzbichler, S. E. Volz, J. Joung, J. van der Oost, A. Regev, E. V. Koonin, F. Zhang, Cpf1 is a single RNA-guided endonuclease of a class 2 CRISPR-Cas system. *Cell* **163**, 759–771 (2015).
15. Y. Kim, S.-A. Cheong, J. G. Lee, S.-W. Lee, M. S. Lee, I.-J. Baek, Y. H. Sung, Generation of knockout mice by Cpf1-mediated gene targeting. *Nat. Biotechnol.* **34**, 808–810 (2016).
16. D. Kim, J. Kim, J. K. Hur, K. W. Been, S.-h. Yoon, J.-S. Kim, Genome-wide analysis reveals specificities of Cpf1 endonucleases in human cells. *Nat. Biotechnol.* **34**, 876–881 (2016).
17. S. Q. Tsai, M. S. Prew, N. T. Nguyen, M. M. Welch, J. M. Lopez, Z. R. McCaw, M. J. Aryee, B. P. Kleinstiver, J. K. Joung, Genome-wide specificities of CRISPR-Cas Cpf1 nucleases in human cells. *Nat. Biotechnol.* **34**, 882–887 (2016).
18. E. Tóth, N. Weinhardt, P. Bencsura, K. Huszár, P. I. Kulcsár, A. Tálas, E. Fodor, E. Welker, Cpf1 nucleases demonstrate robust activity to induce DNA modification by exploiting homology directed repair pathways in mammalian cells. *Biol. Direct* **11**, 46 (2016).
19. M. Jinek, K. Chylinski, I. Fonfara, M. Hauer, J. A. Doudna, E. Charpentier, A programmable dual-RNA-guided DNA endonuclease in adaptive bacterial immunity. *Science* **337**, 816–821 (2012).
20. I. Fonfara, H. Richter, M. Bratovič, A. Le Rhun, E. Charpentier, The CRISPR-associated DNA-cleaving enzyme Cpf1 also processes precursor CRISPR RNA. *Nature* **532**, 517–521 (2016).
21. C. Long, L. Amoasii, A. A. Mireault, J. R. McAnally, H. Li, E. Sanchez-Ortiz, S. Bhattacharyya, J. M. Shelton, R. Bassel-Duby, E. N. Olson, Postnatal genome editing partially restores dystrophin expression in a mouse model of muscular dystrophy. *Science* **351**, 400–403 (2016).
22. C. S. Young, M. R. Hicks, N. V. Ermolova, H. Nakano, M. Jan, S. Younesi, S. Karumbayaram, C. Kumagai-Cresse, D. Wang, J. A. Zack, D. B. Kohn, A. Nakano, S. F. Nelson, M. C. Miceli, M. J. Spencer, A. D. Pyle, A single CRISPR-Cas9 deletion strategy that targets the majority of DMD patients restores dystrophin function in hiPSC-derived muscle cells. *Cell Stem Cell* **18**, 533–540 (2016).
23. L. Xu, K. H. Park, L. Zhao, J. Xu, M. El Refaey, Y. Gao, H. Zhu, J. Ma, R. Han, CRISPR-mediated genome editing restores dystrophin expression and function in *mdx* mice. *Mol. Ther.* **24**, 564–569 (2016).
24. A. Aartsma-Rus, I. Fokkema, J. Verschueren, I. Gijsjaar, J. van Deutkom, G.-J. van Ommen, J. T. den Dunnen, Theoretic applicability of antisense-mediated exon skipping for Duchenne muscular dystrophy mutations. *Hum. Mutat.* **30**, 293–299 (2009).
25. S. Cirak, V. Arechavala-Gomeza, M. Guglieri, L. Feng, S. Torelli, K. Anthony, S. Abbs, M. E. Garralda, J. Bourke, D. J. Wells, G. Dickson, M. J. Wood, S. D. Wilton, V. Straub, R. Kole, S. B. Shrewsbury, C. Sewry, J. E. Morgan, K. Bushby, F. Muntoni, Exon skipping and dystrophin restoration in patients with Duchenne muscular dystrophy after systemic phosphorodiamidate morpholino oligomer treatment: An open-label, phase 2, dose-escalation study. *Lancet* **378**, 595–605 (2011).
26. R. A. Padgett, New connections between splicing and human disease. *Trends Genet.* **28**, 147–154 (2012).
27. P. W. Burridge, E. Matsa, P. Shukla, Z. C. Lin, J. M. Churko, A. D. Ebert, F. Lan, S. Diecke, B. Huber, N. M. Mordwinkin, J. R. Plews, O. J. Abilez, B. Cui, J. D. Gold, J. C. Wu, Chemically defined generation of human cardiomyocytes. *Nat. Methods* **11**, 855–860 (2014).
28. D. P. Millay, M. A. Sargent, H. Osinska, C. P. Baines, E. R. Barton, G. Vuagniaux, H. L. Sweeney, J. Robbins, J. D. Molkentin, Genetic and pharmacologic inhibition of mitochondrial-dependent necrosis attenuates muscular dystrophy. *Nat. Med.* **14**, 442–447 (2008).
29. F. Mourkioti, J. Kustan, P. Kraft, J. W. Day, M.-M. Zhao, M. Kost-Alimova, A. Protopopov, R. A. DePinho, D. Bernstein, A. K. Meeker, H. M. Blau, Role of telomere dysfunction in cardiac failure in Duchenne muscular dystrophy. *Nat. Cell Biol.* **15**, 895–904 (2013).
30. M. Maresca, V. G. Lin, N. Guo, Y. Yang, Obligate ligation-gated recombination (ObLiGaRe): Custom-designed nuclease-mediated targeted integration through nonhomologous end joining. *Genome Res.* **23**, 539–546 (2013).
31. C. Zechner, L. Lai, J. F. Zechner, T. Geng, Z. Yan, J. W. Rumsey, D. Collia, Z. Chen, D. F. Wozniak, T. C. Leone, D. P. Kelly, Total skeletal muscle PGC-1 deficiency uncouples mitochondrial derangements from fiber type determination and insulin sensitivity. *Cell Metab.* **12**, 633–642 (2010).
32. K. K. Baskin, C. E. Grueter, C. M. Kusminski, W. L. Holland, A. L. Bookout, S. Satapati, Y. M. Kong, S. C. Burgess, C. R. Malloy, P. E. Scherer, C. B. Newgard, R. Bassel-Duby, E. N. Olson, MED13-dependent signaling from the heart confers leanness by enhancing metabolism in adipose tissue and liver. *EMBO Mol. Med.* **6**, 1610–1621 (2014).

Acknowledgments: We thank J. Cabrera for assistance with graphics. **Funding:** This work was supported by grants from the NIH (HL130253, HL-077439, DK-099653, and AR-067294), a Paul D. Wellstone Muscular Dystrophy Cooperative Research Center grant (U54 HD 087351), and the Robert A. Welch Foundation (grant 1-0025 to E.N.O.). **Author contributions:** Y.Z., C.L., and E.N.O. designed the project; Y.Z., H.L., J.R.M., K.K.B., and J.M.S. performed the experiments; Y.Z., C.L., R.B.-D., and E.N.O. wrote and edited the manuscript. **Competing interests:** R.B.-D. and E.N.O. are consultants for Exonics Therapeutics. E.N.O., Y.Z., C.L., and R.B.-D. are listed on the patent entitled “Prevention of muscular dystrophy by CRISPR-Cpf1-mediated gene editing” (U.S. Patent 62/426,853, 28 November 2016). The other authors declare that they have no competing interests. **Data and materials availability:** All data needed to evaluate the conclusions in the paper are present in the paper and/or the Supplementary Materials. Additional data related to this paper may be requested from the authors.

Submitted 13 November 2016

Accepted 14 February 2017

Published 12 April 2017

10.1126/sciadv.1602814

Citation: Y. Zhang, C. Long, H. Li, J. R. McAnally, K. K. Baskin, J. M. Shelton, R. Bassel-Duby, E. N. Olson, CRISPR-Cpf1 correction of muscular dystrophy mutations in human cardiomyocytes and mice. *Sci. Adv.* **3**, e1602814 (2017).